





# Isothermal Bondi Accretion in Jaffe and Hernquist Galaxies with a Central Black Hole: Fully Analytical Solutions

Luca Ciotti  and Silvia Pellegrini 

Department of Physics and Astronomy, University of Bologna, via Piero Gobetti 93/2, I-40129 Bologna, Italy; [luca.ciotti@unibo.it](mailto:luca.ciotti@unibo.it)  
Received 2017 June 25; revised 2017 September 6; accepted 2017 September 13; published 2017 October 9

## Abstract

One of the most active fields of research of modern-day astrophysics is that of massive black hole formation and coevolution with the host galaxy. In these investigations, ranging from cosmological simulations, to semi-analytical modeling, to observational studies, the Bondi solution for accretion on a central point-mass is widely adopted. In this work we generalize the classical Bondi accretion theory to take into account the effects of the gravitational potential of the host galaxy, and of radiation pressure in the optically thin limit. Then, we present the fully analytical solution, in terms of the Lambert–Euler  $W$ -function, for isothermal accretion in Jaffe and Hernquist galaxies with a central black hole. The flow structure is found to be sensitive to the shape of the mass profile of the host galaxy. These results and the formulae that are provided, most importantly, the one for the critical accretion parameter, allow for a direct evaluation of all flow properties, and are then useful for the abovementioned studies. As an application, we examine the departure from the true mass accretion rate of estimates obtained using the gas properties at various distances from the black hole, under the hypothesis of classical Bondi accretion. An overestimate is obtained from regions close to the black hole, and an underestimate outside a few Bondi radii; the exact position of the transition between the two kinds of departure depends on the galaxy model.

*Key words:* accretion, accretion disks – galaxies: active – galaxies: elliptical and lenticular, cD – hydrodynamics – X-rays: galaxies – X-rays: ISM

## 1. Introduction

Bondi (1952) presented the solution for spherically symmetric steady accretion of a spatially infinite gas distribution onto an isolated central point-mass. This solution in recent years became a standard and intensively adopted tool for estimates of the scale-radius and the mass flow rate in studies of accretion on massive black holes (hereafter MBHs) at the center of galaxies. In fact, the discovery of the ubiquitous presence of MBHs at the center of spheroids on the one hand (Kormendy & Richstone 1995) and the enormous advance in instrumental capabilities, computer performances, and numerical astrophysics on the other triggered a huge increase in the number of investigations involving the accretion phenomenon at the center of galaxies. These studies range from observational works deriving the gas properties in regions surrounding the MBHs (see, e.g., Baganoff et al. 2003; Pellegrini 2005, 2010; Rafferty et al. 2006; Kormendy & Ho 2013; Wong et al. 2014; Russell et al. 2015), to theoretical studies on the origin of the various types of AGN sources and on the various physical processes involved in accretion onto an MBH (e.g., Bu et al. 2013; Yuan & Narayan 2014; Cao 2016; Park et al. 2017), to cosmological investigations of MBH formation, and coevolution of MBHs and host galaxies involving the “feedback” action (see, e.g., Hopkins et al. 2006, 2007; Sijacki et al. 2007; Di Matteo et al. 2008; Park & Ricotti 2011; Volonteri et al. 2015; Choi et al. 2017; DeGraf et al. 2017). Unfortunately, in general, these studies lack the resolution to follow gas transport down to the parsec scale, and the Bondi model is used as the starting point for estimates of the accretion radius (i.e., the sonic radius) and of the mass accretion rate. In particular, the Bondi accretion rate gives the mass supply to the MBH by taking the density and temperature at some finite distance from the center, implicitly assuming that these values represent the true boundary conditions (i.e., at infinity) for the

Bondi problem. Even the knowledge of the true boundary conditions, however, would not be enough for a proper treatment of the real problem because the MBH is not an isolated point-mass, but resides at the bottom of the potential well of the host galaxy. Moreover, the radiation emitted by the inflowing material may interact with it, accretion may become unsteady, and Bondi accretion during phases of AGN feedback cannot be applied (e.g., Barai et al. 2012; Ciotti & Ostriker 2012). During phases of moderate accretion (in the “maintenance” mode), instead, when the problem can be considered almost steady, Bondi accretion could provide a reliable approximation of the real situation.

In Korol et al. (2016, hereafter KCP16), we generalized the Bondi problem to mass accretion at the center of galaxies, including the effect of electron scattering on the accreting gas as well. We then calculated the deviation from the true values of estimates of the Bondi radius and mass accretion rate due to adopting as boundary values for the density and temperature those at a finite distance from the MBH, and assuming the validity of the classical Bondi accretion solution. In the case of the Hernquist galaxy model, we showed how the analytical expression for the critical value of the accretion parameter  $\lambda_{\text{cr}}$  can be obtained for generic values of the polytropic index  $\gamma$ . However, even for this exceptional case, the radial profiles of the properties of the accreting gas remained to be determined numerically. Of course, in observational studies, or in numerical simulations where subgrid MBH accretion is implemented, analytical solutions for these radial profiles would be very useful. Here we show that, remarkably, the whole accretion problem can be solved in a *fully* analytical way for the *isothermal* accretion in Jaffe (1983) and Hernquist (1990) galaxy models with central MBHs. This is due to the fact that (1) it is possible for these two models to explicitly obtain  $\lambda_{\text{cr}}$ , and (2) the radial profile of the Mach number can be

explicitly written in terms of the *Lambert–Euler W*-function in isothermal accretion in generic spherically symmetric potentials. The possibility of using the *W*-function to describe isothermal flows had been pointed out when discussing the isothermal Parker solution for the solar wind (Cranmer 2004; Waters & Proga (2012); see also Herbst (2015) for the case of accretion). To the best of our knowledge, the present work provides the first fully analytical solution of the accretion problem on an MBH at the center of a galaxy.

This paper is organized as follows. In Section 2 we recall the main properties of the classical Bondi solution, and we present the fully analytical isothermal solution for accretion onto an isolated MBH. In Section 3 we consider the generalized case of the Bondi solution in presence of radiation feedback and of a galaxy potential hosting the central MBH. Section 4 deals with the Jaffe and Hernquist galaxy models, and presents the fully analytical solution for them. In Section 5 we examine the departure of the estimate of the mass accretion rate from the true value, when the estimate is obtained using as boundary values for the density and temperature the values at points along the solution at a finite distance from the MBH. The main conclusions are summarized in Section 6, and technical details are given in the appendixes.

## 2. The Classical Bondi Model

We briefly recall here the main properties of the classical polytropic Bondi accretion model, even though the present investigation focuses on isothermal accretion. The gas is perfect, has a spatially infinite distribution, and is accreting onto an isolated central mass, in our case, an MBH, of mass  $M_{\text{BH}}$ . The gas density and pressure are linked by

$$p = \frac{k_{\text{B}} \rho T}{\mu m_{\text{p}}} = p_{\infty} \tilde{\rho}^{\gamma}, \quad \tilde{\rho} \equiv \frac{\rho}{\rho_{\infty}}, \quad (1)$$

where  $1 \leq \gamma \leq 5/3$  is the polytropic index,  $m_{\text{p}}$  is the proton mass,  $\mu$  is the mean molecular weight,  $k_{\text{B}}$  is the Boltzmann constant, and  $p_{\infty}$  and  $\rho_{\infty}$  are the gas pressure and density at infinity, respectively. The polytropic gas sound speed is

$$c_{\text{s}}^2 = \gamma \frac{p}{\rho}. \quad (2)$$

The isothermal case is recovered for  $\gamma = 1$ . The time-independent continuity equation is

$$4\pi r^2 \rho(r) v(r) = \dot{M}_{\text{B}}, \quad (3)$$

where  $v(r)$  is the gas radial velocity, and  $\dot{M}_{\text{B}}$  is the time-independent accretion rate onto the MBH. The Bernoulli equation, with the appropriate boundary conditions at infinity, becomes

$$\frac{v(r)^2}{2} + \Delta h(r) - \frac{GM_{\text{BH}}}{r} = 0, \quad (4)$$

where, from Equation (1),

$$\Delta h \equiv \int_{p_{\infty}}^p \frac{dp}{\rho} = c_{\infty}^2 \times \begin{cases} \frac{\tilde{\rho}^{\gamma-1} - 1}{\gamma - 1}, & \gamma > 1, \\ \ln \tilde{\rho}, & \gamma = 1, \end{cases} \quad (5)$$

and  $c_{\infty}$  is the sound speed of the gas at infinity.

An important scale length of the problem, the so-called Bondi radius, is naturally defined as

$$r_{\text{B}} \equiv \frac{GM_{\text{BH}}}{c_{\infty}^2}. \quad (6)$$

In the following we use  $r_{\text{B}}$  as given by the definition above as the length scale, even when considering more general models. After introducing the normalized quantities

$$x \equiv \frac{r}{r_{\text{B}}}, \quad \tilde{c}_{\text{s}} \equiv \frac{c_{\text{s}}}{c_{\infty}} = \tilde{\rho}^{\frac{\gamma-1}{2}}, \quad \mathcal{M} = \frac{v}{c_{\text{s}}}, \quad (7)$$

where  $\mathcal{M}$  is the Mach number, Equations (3)–(4) become respectively

$$x^2 \mathcal{M} \tilde{\rho}^{\frac{\gamma+1}{2}} = \frac{\dot{M}_{\text{B}}}{4\pi r_{\text{B}}^2 \rho_{\infty} c_{\infty}} \equiv \lambda, \quad (8)$$

$$\begin{cases} \frac{\mathcal{M}^2 \tilde{c}_{\text{s}}^2}{2} + \frac{\tilde{\rho}^{\gamma-1}}{\gamma-1} = \frac{1}{x} + \frac{1}{\gamma-1}, & \gamma > 1, \\ \frac{\mathcal{M}^2 \tilde{c}_{\text{s}}^2}{2} + \ln \tilde{\rho} = \frac{1}{x}, & \gamma = 1. \end{cases} \quad (9)$$

$\lambda$  is the dimensionless accretion parameter that determines the accretion rate for assigned  $M_{\text{BH}}$  and boundary conditions. From Equations (7)–(8), the radial profile of all hydrodynamical properties can be expressed in terms of  $\mathcal{M}(x)$ . By elimination of  $\tilde{\rho}$  in Equations (8)–(9) for  $1 < \gamma \leq 5/3$ , the Bondi problem reduces to the solution of the equation

$$g(\mathcal{M}) = \Lambda f(x), \quad \Lambda \equiv \lambda^{\frac{2(1-\gamma)}{\gamma+1}}, \quad (10)$$

where

$$g(\mathcal{M}) \equiv \mathcal{M}^{\frac{2(1-\gamma)}{\gamma+1}} \left( \frac{\mathcal{M}^2}{2} + \frac{1}{\gamma-1} \right), \quad (11)$$

and

$$f(x) \equiv x^{\frac{4(\gamma-1)}{\gamma+1}} \left( \frac{1}{x} + \frac{1}{\gamma-1} \right). \quad (12)$$

As is well known,  $\Lambda$  cannot be chosen arbitrarily; in fact, both  $g(\mathcal{M})$  and  $f(x)$  have a minimum:

$$g_{\text{min}} = \frac{\gamma+1}{2(\gamma-1)}, \quad \text{for } \mathcal{M}_{\text{min}} = 1, \quad (13)$$

and

$$f_{\text{min}} = \frac{\gamma+1}{4(\gamma-1)} \left( \frac{4}{5-3\gamma} \right)^{\frac{5-3\gamma}{\gamma+1}}, \quad \text{for } x_{\text{min}} = \frac{5-3\gamma}{4}. \quad (14)$$

Therefore, to satisfy Equation (10)  $\forall x > 0$  requires that  $g_{\text{min}} \leq \Lambda f_{\text{min}}$ , i.e., that  $\Lambda \geq \Lambda_{\text{cr}} \equiv g_{\text{min}}/f_{\text{min}}$ . In order for the solution to exist, it is then required that

$$\lambda \leq \lambda_{\text{cr}} = \left( \frac{f_{\text{min}}}{g_{\text{min}}} \right)^{\frac{\gamma+1}{2(\gamma-1)}} = \frac{1}{4} \left( \frac{2}{5-3\gamma} \right)^{\frac{5-3\gamma}{2(\gamma-1)}}. \quad (15)$$

In particular,  $\lambda_{\text{cr}} = e^{3/2}/4$  for  $\gamma \rightarrow 1^+$ , and  $\lambda_{\text{cr}} = 1/4$  for  $\gamma \rightarrow 5/3^-$ .

In the isothermal case, the Bondi problem is given by

$$\begin{cases} g(\mathcal{M}) = f(x) - \Lambda, & \Lambda \equiv \ln \lambda, \\ g(\mathcal{M}) \equiv \frac{\mathcal{M}^2}{2} - \ln \mathcal{M}, \\ f(x) \equiv \frac{1}{x} + 2 \ln x, \end{cases} \quad (16)$$

with

$$\begin{cases} g_{\min} = \frac{1}{2}, & \text{for } \mathcal{M}_{\min} = 1, \\ f_{\min} = 2 - 2 \ln 2, & \text{for } x_{\min} = \frac{1}{2}, \end{cases} \quad (17)$$

so that solutions exist only for  $g_{\min} \leq f_{\min} - \Lambda$ , i.e., for  $\Lambda \leq \Lambda_{\text{cr}} \equiv f_{\min} - g_{\min}$ . Equation (16) then requires

$$\lambda \leq \lambda_{\text{cr}} = e^{f_{\min} - g_{\min}} = \frac{e^{3/2}}{4}, \quad (18)$$

in accordance with the limit of Equation (15) for  $\gamma \rightarrow 1^+$ . In the following, the function  $f(x)$  in Equation (16) is generalized by considering the effect of radiation pressure due to electron scattering, and the additional gravitational field of the host galaxy.

Summarizing, the solution of the Bondi problem requires obtaining the radial profile  $\mathcal{M}(x)$  for given  $\lambda \leq \lambda_{\text{cr}}$  (see, e.g., Bondi 1952; Frank et al. 1992). Unfortunately, Equation (10) does not have an explicit solution in terms of known functions for generic values of  $\gamma$ , and must be solved numerically.

### 2.1. The Isothermal Solution

Of the two critical solutions characterizing the Bondi problem, we consider the solution pertinent to accretion, with an increasing Mach number approaching the center. Appendix A shows that by introducing the Lambert–Euler function  $W$  and using Equation (54) with  $a = 1/2$ ,  $b = 2$ ,  $c = 0$ ,  $d = -1$ ,  $X = \mathcal{M}$  and  $Y = f(x) - \Lambda$ , one can solve Equation (16) for  $\mathcal{M}(x)$ , and then recover the full solution for isothermal accretion (see also Waters & Proga 2012). In particular, along the critical solution, when  $\lambda = \lambda_{\text{cr}}$ ,  $\mathcal{M}^2$  is given by

$$\mathcal{M}^2 = - \begin{cases} W\left(0, -\frac{e^{3-2/x}}{16x^4}\right), & x \geq x_{\min}, \\ W\left(-1, -\frac{e^{3-2/x}}{16x^4}\right), & 0 < x \leq x_{\min}, \end{cases} \quad (19)$$

where  $x_{\min} = 1/2$  (Equation (17)).

The properties of the critical solution (19) can be visualized with the help of Figure 5 in Appendix A. Figure 5 shows that only for a negative argument,  $W$  assumes negative values, and so  $\mathcal{M}^2$  can be a positive quantity. As  $x$  decreases from infinity to the sonic point  $x_{\min} = 1/2$ , the argument  $z$  of the  $W(0, z)$  function decreases from 0 to  $-1/e$ , and the function  $W(0, z)$  decreases from 0 to  $-1$ , i.e., from point A to point B (solid line in Figure 5). Then, when  $x$  decreases further, approaching the origin, the argument of the branch  $W(-1, z)$  increases again from  $-1/e$  to 0, and  $W$  decreases from  $-1$  to  $-\infty$ , moving from point B to the asymptotic point C (dashed line in Figure 5). Note that the  $W(-1, z)$  function describes

supersonic accretion, while  $W(0, z)$  describes subsonic accretion, so that the critical solution is obtained by connecting the two branches. This is illustrated by the red and blue solid lines, respectively, in Figure 1. Note also that in case of isothermal accretion with  $\lambda < \lambda_{\text{cr}}$ , the continuous solutions are limited to a subset of the regions A–B (the subsonic accretion branch, blue dotted lines), or to a subset of the region B–C (the supersonic accretion branch, red dotted lines).

After obtaining  $\mathcal{M}(x)$  from Equation (8) with  $\gamma = 1$ , one has

$$\tilde{\rho}(x) = \frac{\lambda_{\text{cr}}}{x^2 \mathcal{M}(x)}, \quad (20)$$

while the modulus of the accretion velocity is  $v(r) = c_{\infty} \mathcal{M}(x)$ .

## 3. Generalized Bondi Accretion for an Isothermal Flow

### 3.1. Adding the Effect of Electron Scattering

The Bondi solution describes a purely hydrodynamical flow, where heat exchanges are implicitly taken into account by the polytropic index<sup>1</sup> (see also KCP16, Section 3). In real cases, the flow can be affected by the emission of radiation near the MBH; in terms of the mass accretion rate  $\dot{M}_{\text{acc}}$ , this is expressed by

$$L = \varepsilon \dot{M}_{\text{acc}} c^2, \quad (21)$$

where  $\varepsilon$  is the radiative efficiency. For example, in the classical Bondi accretion, one would adopt  $\dot{M}_{\text{acc}} = \dot{M}_{\text{B}}$ . The efficiency  $\varepsilon$  can depend on  $\dot{M}_{\text{acc}}$ , as in the advection dominated accretion at low  $\dot{M}_{\text{acc}}$  (e.g., Yuan & Narayan 2014), when  $\varepsilon$  is very low. At high accretion rates, the efficiency is instead  $\varepsilon_0 \simeq 0.1$ , and the effects of the emitted radiation can be sufficiently strong to stop accretion; in these circumstances, the steady Bondi solution cannot be applied, not even approximately (e.g., Ciotti & Ostriker 2012 for a review; Barai et al. 2012).

KCP16 extended the classical Bondi accretion solution by including the radiation pressure effect due to electron scattering in the optically thin regime (see also Fukue 2001; Lusso & Ciotti 2011). Under the assumption of spherical symmetry, the total (gravity plus radiation) force on a gas element is

$$F(r) = -\frac{GM_{\text{BH}}\rho(r)\chi}{r^2}, \quad \chi \equiv 1 - l, \quad l \equiv \frac{L}{L_{\text{Edd}}}, \quad (22)$$

where  $L_{\text{Edd}} = 4\pi c GM_{\text{BH}} \bar{m}_{\text{p}} / \sigma_{\text{T}}$  is the Eddington luminosity, and  $\sigma_{\text{T}} = 6.65 \times 10^{-25} \text{ cm}^2$  is the Thomson cross section. When  $L = L_{\text{Edd}}$ , and then  $\chi = 0$ , radiation pressure cancels exactly the MBH gravitational field at all radii; when  $\chi = 1$ , the radiation pressure has no effect on the accretion flow. We define  $\dot{M}_{\text{es}}$  as the accretion rate under the above hypotheses; then, in terms of the Eddington mass accretion rate  $\dot{M}_{\text{Edd}}$ , one has

$$\dot{M}_{\text{Edd}} \equiv \frac{L_{\text{Edd}}}{\varepsilon_0 c^2}, \quad l = \frac{\dot{M}_{\text{es}} \varepsilon}{\dot{M}_{\text{Edd}} \varepsilon_0}. \quad (23)$$

As demonstrated by KCP16, the value of  $L_{\text{Edd}}$  to be inserted in Equations (22) and (23) remains the value corresponding to the

<sup>1</sup>  $\gamma$  is not necessarily the adiabatic index  $\gamma_{\text{ad}}$ , so that in the Bondi solution, the entropy of the gas can change along the radial streamlines. For a polytropic transformation of specific heat at constant volume  $\mathcal{C}_V$ , the molar specific heat is  $\mathcal{C} = \mathcal{C}_V(\gamma_{\text{ad}} - \gamma)/(1 - \gamma)$  (e.g., Chandrasekhar 1939). Therefore  $\mathcal{C} < 0$  when  $1 < \gamma < \gamma_{\text{ad}}$ , and the fluid element loses energy as it moves inward and heats.

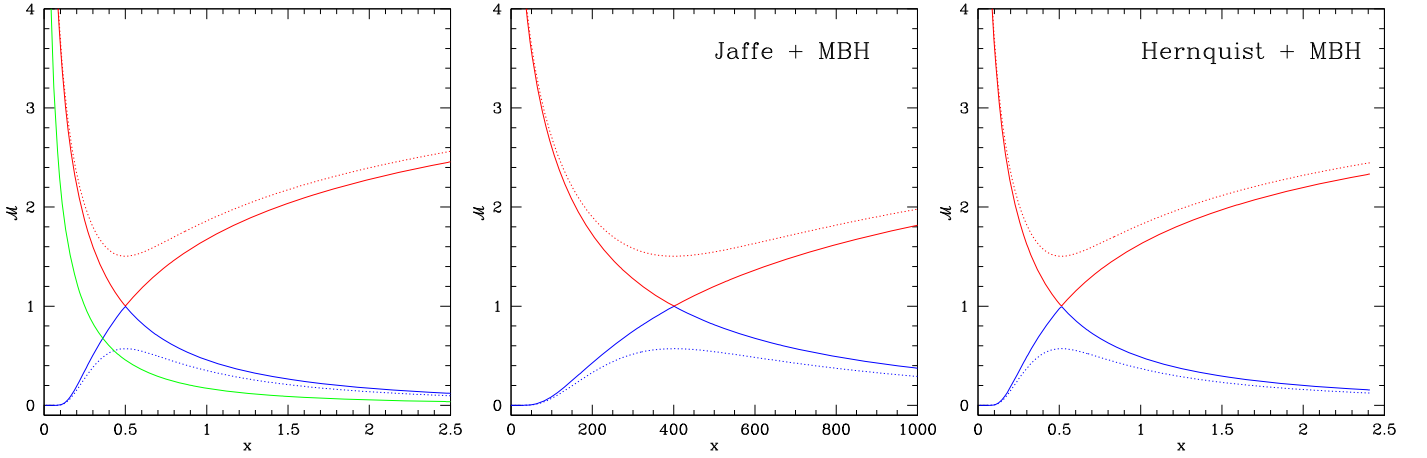


**Figure 1.** Mach number profile  $\mathcal{M}(x)$  for isothermal Bondi accretion on an MBH. Blue lines show the subsonic regime, red lines the supersonic regime. The leftmost panel refers to classical Bondi accretion (Section 2.1), and the green line refers to the inclusion of the effect of radiation pressure for  $\chi = 0.5$  (Section 3.1). The middle and right panels show accretion at the center of a Jaffe and a Hernquist galaxy model, respectively, with  $\mathcal{R} = 1000$ ,  $\xi = 100$  and  $\chi = 1$  (Sections 4.1 and 4.2). Solid lines show the two critical solutions, one in which  $\mathcal{M}$  continuously increases toward the center, and the other in which the flow starts supersonic and reaches the center with zero velocity. The dotted lines show the illustrative example of the two subcritical solutions with  $\lambda = 0.8\lambda_{\text{cr}}$ . Note that for this particular choice of the  $\mathcal{R}$  and  $\xi$  values, the position of the sonic point moves considerably outward in presence of a Jaffe galaxy (Section 4.1); for the Hernquist galaxy, the sonic point is instead similar to that of the classical Bondi accretion, that is, it remains small (Section 4.2).

gravity produced only by the MBH, even when the gravitational potential of the host galaxy is also present.

The radiation feedback can be implemented as a correction that reduces the effective gravitational force of the MBH by the factor  $\chi$ . In particular, for  $\gamma = 1$  the function  $f$  in Equation (16) becomes

$$f(x) = \frac{\chi}{x} + 2 \ln x, \quad (24)$$

and the position of the minimum of the new  $f$  moves inward with respect to the classical case:

$$x_{\text{min}} = \frac{\chi}{2}. \quad (25)$$

From the value of  $x_{\text{min}}$  and  $f_{\text{min}} = f(x_{\text{min}})$ , one derives the critical value of the accretion parameter, which we now call  $\lambda_{\text{es}}$ :

$$\lambda_{\text{es}} = \chi^2 \lambda_{\text{cr}}, \quad (26)$$

where  $\lambda_{\text{cr}}$  is the critical parameter in the corresponding classical case. In turn, the new accretion rate,  $\dot{M}_{\text{es}}$ , is reduced with respect to  $\dot{M}_{\text{B}}$ , for a given  $M_{\text{BH}}$  and boundary conditions at infinity:

$$\dot{M}_{\text{es}} = 4\pi r_{\text{B}}^2 \lambda_{\text{es}} \rho_{\infty} c_{\infty} = \frac{\lambda_{\text{es}}}{\lambda_{\text{cr}}} \dot{M}_{\text{B}} = \chi^2 \dot{M}_{\text{B}}. \quad (27)$$

The equation above is an implicit equation for  $\dot{M}_{\text{es}}$  because  $\chi$  depends on  $\dot{M}_{\text{es}}$  itself through Equations (22)–(23). It can be shown that  $\dot{M}_{\text{es}}$  self-regulates, and cannot exceed  $\dot{M}_{\text{Edd}}$ , regardless of the size of  $\dot{M}_{\text{B}}$  (see KCP16 for a more detailed discussion).

We then use the same procedure as in Section 2.1 to derive the Mach profile of the critical isothermal solution for generic values of  $\chi$ ;  $\mathcal{M}(x)$  is now given by

$$\mathcal{M}^2 = - \begin{cases} W\left(0, -\frac{\chi^4 e^{3-2\chi/x}}{16x^4}\right), & x \geq x_{\text{min}}, \\ W\left(-1, -\frac{\chi^4 e^{3-2\chi/x}}{16x^4}\right), & 0 < x \leq x_{\text{min}}, \end{cases} \quad (28)$$

where now  $x_{\text{min}} = \chi/2$ . In Figure 1 (left panel), the green line compares the  $\mathcal{M}$  profile of the critical solution with that of the classical Bondi problem for the illustrative case  $\chi = 0.5$ ; as dictated by Equation (25), the sonic radius moves inward, with  $x_{\text{min}} = 1/4$ . The density profile, setting  $\gamma = 1$  in Equation (8), becomes

$$\tilde{\rho}(x) = \frac{\lambda_{\text{es}}}{x^2 \mathcal{M}(x)}. \quad (29)$$

### 3.2. Adding the Potential of the Galaxy

We now move to the most general problem of Bondi accretion with electron scattering in the potential of the galaxy hosting the MBH at its center. We write the gravitational potential of a spherical galaxy of finite total mass  $M_{\text{g}}$  as

$$\phi_{\text{g}} = -\frac{GM_{\text{g}}}{r_{\text{g}}} \psi\left(\frac{r}{r_{\text{g}}}\right), \quad (30)$$

where  $r_{\text{g}}$  and  $\psi$  are a characteristic scale length and the dimensionless galaxy potential, respectively. We assume that  $\psi = 0$  for  $r \rightarrow \infty$ , so that the Bernoulli constant in Equation (4) can still be fixed at infinity. We further introduce the parameters

$$\mathcal{R} \equiv \frac{M_{\text{g}}}{M_{\text{BH}}}, \quad \xi \equiv \frac{r_{\text{g}}}{r_{\text{B}}}, \quad (31)$$

with which the effective total potential becomes

$$\phi_{\text{t}} = -\frac{GM_{\text{BH}}}{r_{\text{B}}} \left[ \frac{\chi}{x} + \frac{\mathcal{R}}{\xi} \psi\left(\frac{x}{\xi}\right) \right]. \quad (32)$$

The function  $f(x)$  in Equation (16) is now written as

$$f = \frac{\chi}{x} + \frac{\mathcal{R}}{\xi} \psi\left(\frac{x}{\xi}\right) + 2 \ln x. \quad (33)$$

Therefore the values of  $x_{\text{min}}$ ,  $f_{\text{min}}$ , and of the critical accretion parameter (that we now call  $\lambda_{\text{t}}$ ) depend on  $(\chi, \mathcal{R}, \xi)$ , while the

function  $g(\mathcal{M})$  is unaffected by the addition of the galaxy potential. Note that for  $\mathcal{R} \rightarrow 0$  (or  $\xi \rightarrow \infty$ ), the galaxy contribution vanishes,  $\lambda_t = \lambda_{es}$ , and one recovers the solution of Section 3.1. In the limiting case of  $\chi = 0$ , the problem reduces to Bondi accretion in the potential of the galaxy only, without electron scattering and MBH.

The presence of a galaxy changes the accretion rate, which we now call  $\dot{M}_t$ ; Equation (8) still holds, with

$$\dot{M}_t = 4\pi r_B^2 \lambda_t \rho_\infty c_\infty = \frac{\lambda_t}{\lambda_{cr}} \dot{M}_B, \quad (34)$$

where again  $\dot{M}_B$  is the classical Bondi accretion rate for the same chosen boundary conditions  $\rho_\infty$  and  $c_\infty$ .

The radial trend of the Mach number for the critical solution can be derived again along the lines described in Section 2.1; we now have

$$\mathcal{M}^2 = - \begin{cases} W(0, -e^{-2f+2\Lambda_t}), & x \geq x_{\min} \\ W(-1, -e^{-2f+2\Lambda_t}), & 0 < x \leq x_{\min}, \end{cases} \quad (35)$$

where  $\Lambda_t = \ln \lambda_t = f_{\min} - g_{\min}$  as explained in Section 2. Finally, we have

$$\tilde{\rho}(x) = \frac{\lambda_t}{x^2 \mathcal{M}(x)}. \quad (36)$$

The full solution is then known, provided  $x_{\min}$  is known. For a generic galaxy model,  $x_{\min}$ ,  $f_{\min}$ , and  $\lambda_t$  can be determined only numerically. Moreover, the galaxy potential can produce more than one minimum for  $f(x)$  (KCP16). As we will see in the next section, two of the most common galaxy models remarkably allow for an analytical expression for  $x_{\min}$  and  $\Lambda_t$  in the isothermal case; therefore, *together with the expression above for  $\mathcal{M}$* , we have a fully analytical solution of isothermal accretion on MBHs at the center of such galaxies.

Note that in the critical solution, the argument of the exponential in Equation (35) is  $-2(f - f_{\min}) - 1$ ; thus, as  $x$  decreases from infinity to  $x_{\min}$ , the argument  $z$  decreases from 0 to  $-1/e$ , and the  $W$ -function moves from  $A$  to  $B = (-1/e, -1)$  in Figure 5 of Appendix A, corresponding to the sonic point. Decreasing  $x$  further, the solution switches on the  $W(-1, z)$  branch, and the Mach number diverges at the center. For  $\Lambda < \Lambda_t$ , the subsonic and supersonic cases are again described by the  $W(0, z)$  and  $W(-1, z)$  branches, respectively.

#### 4. Two Fully Analytical Cases: Jaffe and Hernquist Galaxy Models with a Central MBH

In this section we present the final goal of our investigation, the analytical solution for all quantities describing accretion in the isothermal case, for two particular galaxy models, the Hernquist (1990) and the Jaffe (1983) models with a central MBH. These density profiles describe the mass distribution of early-type galaxies well; they belong to the widely used family of the so-called  $\gamma$ -models (Dehnen 1993; Tremaine et al. 1994), which all have similar  $\sim r^{-4}$  density profiles in their external regions (outside  $r_g$ ). For example, the Hernquist model with a central MBH has been adopted in hydrodynamical simulations of Bondi accretion in galaxies (Barai et al. 2011; Park et al. 2016). As already noted,  $\lambda_t$  is known once the *absolute* minimum  $f_{\min}(\chi, \mathcal{R}, \xi)$  is known; this in turn requires the determination of  $x_{\min}(\chi, \mathcal{R}, \xi)$ . Quite remarkably, for the Hernquist model  $x_{\min}$  can be derived analytically in the general

polytropic case, solving a cubic equation (KCP16). A peculiar property of this equation is the possibility to present *two* minima for  $x > 0$ , depending on the galaxy parameters; KCP16 provided the formulae needed to determine the critical points of  $f$  for any choice of  $\gamma$  and of the galaxy parameters, but the final expressions for  $x_{\min}$  and  $f_{\min}$  were not given. Here we give these analytical expressions for  $x_{\min}$  and  $f_{\min}$  in case of isothermal accretion. In addition, we show that  $\lambda_t$  can also be evaluated explicitly for isothermal accretion in the Jaffe model; to our knowledge, these are the only two known cases of fully solvable accretion problems. As we will see, the Jaffe case is simpler than the Hernquist case; this is not unexpected because the Jaffe gravitational potential is logarithmic, like the term appearing in the expression for  $f$  in Equation (33). In practice,  $f$  has only one minimum for all values of the galaxy parameters. For this reason, we begin the discussion with the Jaffe model.

##### 4.1. The Jaffe Model

The gravitational potential of the Jaffe (1983) density distribution is given by

$$\phi_g = \frac{GM_g}{r_g} \ln \left( \frac{r}{r + r_g} \right), \quad (37)$$

where the scale length  $r_g$  is related to the galaxy effective radius  $R_e$  as  $r_g \simeq R_e/0.7447$ . From Equation (37),  $f$  in Equation (33) becomes

$$f = \frac{\chi}{x} - \frac{\mathcal{R}}{\xi} \ln \left( \frac{x}{x + \xi} \right) + 2 \ln x. \quad (38)$$

In three cases the determination of  $x_{\min}$  and  $f_{\min}$  is trivial. First, when  $\xi \rightarrow \infty$  (or  $\mathcal{R} \rightarrow 0$ ), the galaxy contribution vanishes, and the results in Section 3.1 are recovered. Second, although  $\phi_g$  is not continuous at the origin, by fixing  $r > 0$  and considering the limit  $r_g \rightarrow 0$ , the resulting potential is that of an MBH of mass  $M_g$ ; thus, this limiting case reduces to the problem of accretion on an MBH of total (effective) mass  $(\chi + \mathcal{R})M_{\text{BH}}$ , and can be treated as in Section 3.1. In particular, the position of the only minimum of  $f$  (i.e., of the sonic radius) and the critical value  $\lambda_t$  are given by

$$x_{\min} = \frac{\chi + \mathcal{R}}{2}, \quad \lambda_t = (\chi + \mathcal{R})^2 \lambda_{cr}, \quad (39)$$

where  $\lambda_{cr}$  is the critical value for the corresponding classical Bondi problem (Section 2). Third, for  $\chi = 0$ , the discussion in Appendix B shows that isothermal accretion in the Jaffe potential is possible only for  $\mathcal{R} \geq 2\xi$ ; this condition is equivalent to the requirement that  $GM_g \geq 2r_g c_\infty^2$ . We derive for  $x_{\min}$  and  $\lambda_t$  the expressions

$$x_{\min} = \frac{\mathcal{R} - 2\xi}{2}, \quad \lambda_t = \frac{\mathcal{R}^2}{4\sqrt{e}} \left( 1 - \frac{2\xi}{\mathcal{R}} \right)^{2-\mathcal{R}/\xi}. \quad (40)$$

This is equivalent to having  $r_{\min}/r_g = GM_g/(2c_\infty^2 r_g) - 1$ ; for  $\mathcal{R} = 2\xi$ , one has that  $x_{\min} = 0$  and  $\lambda_t = \xi^2/\sqrt{e}$ .

The general expression for  $x_{\min}$  for assigned  $\chi$ ,  $\mathcal{R}$ , and  $\xi$  is given in Equation (56); from this expression,  $f_{\min}$  can be easily evaluated. In Appendix B we also show that there is only one minimum at  $x \geq 0$ . Figure 2 shows the trend of  $x_{\min}$  and  $\lambda_t$  with  $\xi$  for representative values of  $\mathcal{R}$  and  $\chi = 1$ . To facilitate

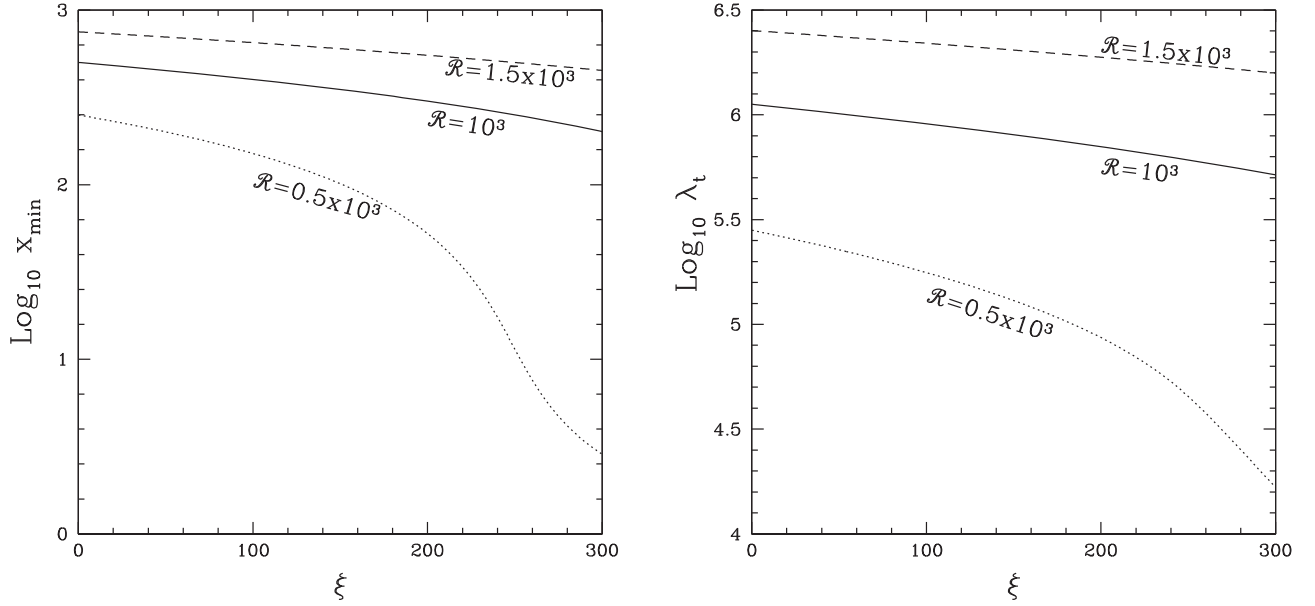


**Figure 2.** Left: position of the sonic point for isothermal accretion in a Jaffe galaxy model as a function of  $\xi$ . The curves have been determined using Equation (56) and refer to a ratio of galaxy mass to MBH mass of  $\mathcal{R} = 500$  (dotted), 1000 (solid), and 1500 (dashed);  $\chi = 1$  is assumed. Right: corresponding values of  $\lambda_t$ , determined following Equation (18), with  $g_{\min} = 1/2$  and with  $f_{\min}$  calculated using Equation (38) for  $x = x_{\min}$ .

inspection of the figure, we recall that the choice of  $\mathcal{R} = 1000$  corresponds to the standard assumption about the ratio between the stellar mass and the MBH mass in spheroids (e.g., Magorrian et al. 1998); a value of  $\xi \approx 100$  is representative of the case of hot gas accretion at the center of elliptical galaxies, when  $r_g$  is a few kpc, and  $r_B$  is on the order of a few tens of pc (e.g., Pellegrini 2010; see also Section 6). Figure 2 shows that  $x_{\min}$  for accretion in the Jaffe potential is much larger than in the classic Bondi solution ( $x_{\min} = 1/2$ ); for reasonable  $\xi \approx 100$  and  $\mathcal{R} \approx 10^3$  (see above),  $x_{\min}$  reaches values of a few hundreds. This significant increase is explained by the compactness of the mass distribution that is typical of the Jaffe model. The critical  $\lambda_t$  is also much larger than in the classical Bondi accretion (Section 2). In the limiting case of  $\xi \rightarrow 0$ , the sonic radius  $x_{\min}$  becomes very large in a way predicted by Equation (39); this same equation also explains the trend for  $\lambda_t \sim \mathcal{R}^2$  shown at low  $\xi$  in the right panel of Figure 2. At large  $\xi$ , the effect of the gravitational field of the galaxy instead diminishes, and correspondingly,  $x_{\min}$  decreases toward the limiting case of classical Bondi accretion; the same is true for  $\lambda_t$ , which tends to  $\lambda_{\text{cr}}$ . Finally, cases with  $\chi < 1$  are not shown in Figure 2 since their differences with the plotted curves are very small and would be appreciated only for very high values of  $\xi$  (or low values of  $\mathcal{R}$ ), i.e., if the gravitational field at the sonic radius is dominated by the presence of the MBH (see Equation (33)).

The critical isothermal solution is given by

$$\mathcal{M}^2 = - \begin{cases} W \left[ 0, -\frac{e^{2f_{\min} - \frac{2\chi}{x}} \left( \frac{x}{x+\xi} \right)^{\frac{2\mathcal{R}}{\xi}}}{e x^4} \right], & x \geq x_{\min}, \\ W \left[ -1, -\frac{e^{2f_{\min} - \frac{2\chi}{x}} \left( \frac{x}{x+\xi} \right)^{\frac{2\mathcal{R}}{\xi}}}{e x^4} \right], & 0 < x \leq x_{\min}. \end{cases} \quad (41)$$

An illustrative solution for the above  $\mathcal{M}(x)$  is given in Figure 1 (middle panel) for the typical values of  $\mathcal{R} = 1000$  and  $\xi = 100$ , and for  $\chi = 1$ . The choice of  $\chi = 1$  means no effect from the radiation pressure, thus Figure 1 (as Figure 2 just discussed) shows purely gravitational effects due to the galactic + MBH potentials; however, as is the case for  $x_{\min}$  and  $\lambda_t$  in Figure 2, the differences in the trend of  $\mathcal{M}$  for  $\chi < 1$  from those shown in Figure 1 would be noticed only for very large  $\xi$ , or very small  $\mathcal{R}$ .

#### 4.2. The Hernquist Model

The gravitational potential of the Hernquist model is

$$\phi_g = -\frac{GM_g}{r + r_g}, \quad (42)$$

where  $r_g \simeq R_e/1.82$ ; thus, from Equation (33), one has

$$f = \frac{\chi}{x} + \frac{\mathcal{R}}{x + \xi} + 2 \ln x. \quad (43)$$

As for the Jaffe model, from the expression above, one sees that in three cases the determination of  $x_{\min}$  and  $f_{\min}$  is trivial. First, when  $\xi \rightarrow \infty$  (or  $\mathcal{R} \rightarrow 0$ ), the galaxy contribution to  $f$  vanishes, and the results of Section 3.1 are recovered. Second, for  $r > 0$  and  $r_g \rightarrow 0$ ,  $\phi_g$  reduces to the potential of an MBH of mass  $M_g$ , and the solution of Section 3.1 applies; for an MBH of total (effective) mass  $(\chi + \mathcal{R})M_{\text{BH}}$ , and Equation (39) gives the position of  $x_{\min}$ . Third, for  $\xi > 0$  and  $\chi = 0$ , at variance with the case of the Jaffe model, no accretion is possible because the minimum of  $f$  is attained for  $x \rightarrow 0^+$ , with  $f_{\min} \rightarrow -\infty$ , and so formally,  $\lambda_t = 0$  is needed. Therefore, from now on we assume  $\xi > 0$  and  $\chi > 0$ .

The procedure to determine  $x_{\min}$  analytically for assigned  $\chi$ ,  $\mathcal{R}$ , and  $\xi$  is given in Appendix B. More than one sonic point can be present; the search for the absolute minimum  $x_{\min}$  can then be difficult. In turn, the profile  $\mathcal{M}(x)$  of the critical

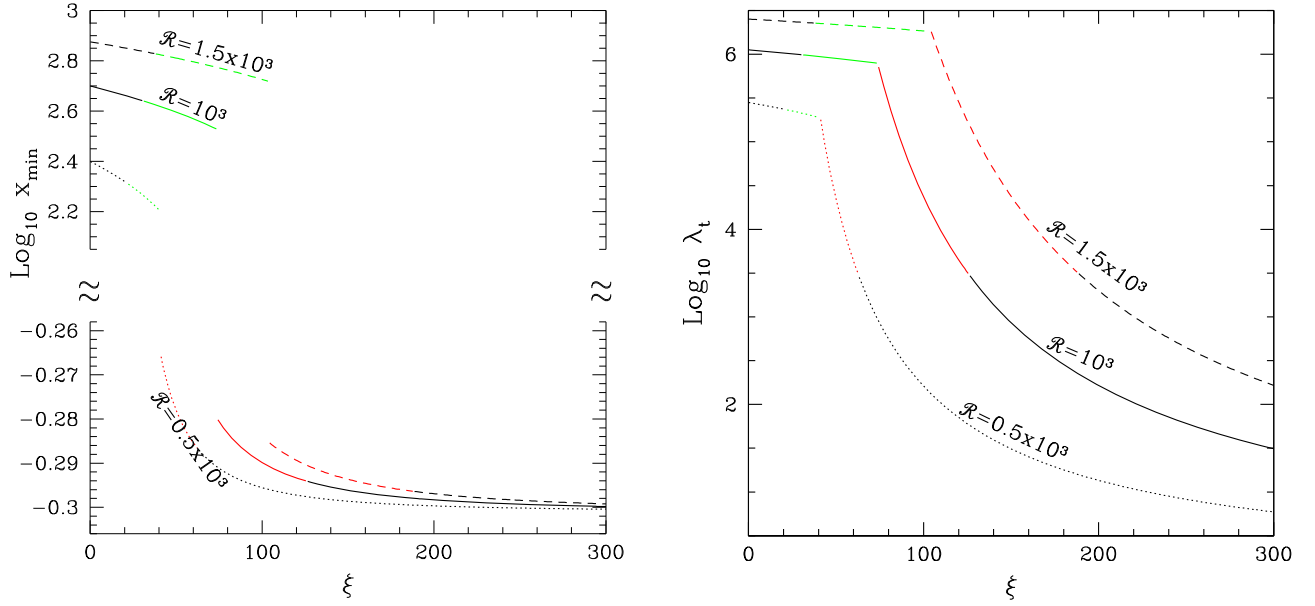


**Figure 3.** Left: position of the sonic point for isothermal accretion in a Hernquist galaxy model as a function of  $\xi$  for  $\chi = 1$ . The curves refer to a ratio of galaxy mass to MBH mass of  $\mathcal{R} = 500$  (dotted), 1000 (solid), and 1500 (dashed). The values of  $x_{\min}$  have been determined using the procedure in Appendix B. The black lines (at low and high values of  $\xi$ ) correspond to the single minimum (see Figure 6 in Appendix B, at fixed  $\mathcal{R}$ ); the green and red lines show  $x_{\min}$  when there are two minima, and they correspond to the solution labeled with  $k = 1$  and  $k = 0$ , respectively, in Appendix B. The jump from the green to the red solution takes place at the value of  $\xi$  such that the two minima of  $f$  have the same value (dotted line in Figure 6 in Appendix B); for a further increase of  $\xi$ ,  $x_{\min}$  switches into the inner region. See Section 4.2 for more details. Right: corresponding values of  $\lambda_t$ ; note that  $\lambda_t$  is a continuous function of  $\xi$ .

solution can be non-monotonic. When  $x_{\min}$  is determined, one can derive  $f_{\min}$ , and then evaluate  $\lambda_t$ . The critical isothermal solution is then

$$\mathcal{M}^2 = - \begin{cases} W \left( 0, -\frac{e^{2f_{\min} - \frac{2\mathcal{R}}{x+\xi} - \frac{2\chi}{x}}}{e^{x^4}} \right), & x \geq x_{\min}, \\ W \left( -1, -\frac{e^{2f_{\min} - \frac{2\mathcal{R}}{x+\xi} - \frac{2\chi}{x}}}{e^{x^4}} \right), & 0 < x \leq x_{\min}. \end{cases} \quad (44)$$

Representative trends for  $x_{\min}$  and  $\lambda_t$  are plotted in Figure 3 as a function of  $\xi$  for three values of  $\mathcal{R}$ , and for  $\chi = 1$ . The parameters are the same as chosen for the Jaffe model in Figure 2, but the trends are very different; the difference is due to the fact that there can be one or three critical points for  $f$  (two minima and one maximum), as discussed in Appendix B. The curves in Figure 3 refer to the absolute minimum. This different behavior is quite surprising, since both the Jaffe and Hernquist models belong to the class of  $\gamma$ -models and are quite similar (for example, in projection, they are both good approximations of the de Vaucouleurs surface brightness profile over a large radial range). The only major difference is that the model density in the central regions goes as  $r^{-2}$  in the Jaffe case, and as  $r^{-1}$  in the Hernquist case.

The left panel shows that  $x_{\min}$  can vary largely. The easiest way to understand this trend is to refer to Figure 6 in Appendix B, at a fixed  $\mathcal{R}$ , and moving from left to right. First we consider the black lines in Figure 3, left panel, that populate low and high  $\xi$  values; in these cases, there is a *single* minimum for  $f$ . In fact, for given  $\mathcal{R}$  and sufficiently small or large  $\xi$ , there is a single minimum, according to Figure 6. In particular, for very small  $\xi$ , the only minimum is placed at very large radii, in accordance with Equation (39); this explains the high values of  $x_{\min}$  in Figure 3. When  $\xi$  increases, the depth of the galactic potential well becomes shallower, and  $x_{\min}$  shifts towards inner

radii. The transition from black to green lines corresponds to the appearance of the three critical points; the  $\xi$ ,  $\mathcal{R}$  values are placed within the triangular region in Figure 6, where there are two minima for  $f$ . The additional new minimum of  $f$  appears close to the center, but the absolute minimum is still at larger radii, even if  $x_{\min}$  is decreasing; thus, the green curves show a decreasing trend with  $\xi$  and correspond to the positions of  $x_{\min}$  given by Equation (67) for  $k = 0$ . As  $\xi$  increases further, the external absolute minimum continues to move toward the center, while the value of  $f$  corresponding to the inner critical point ( $k = 1$  in Equation (67)) continues to decrease. When the  $\xi$ ,  $\mathcal{R}$  values hit the dotted line in Figure 6, the values of  $f$  at the two minima become equal, and then the accretion flow develops two sonic points. One point is very close to the MBH, the other is at much larger radii. As  $\xi$  increases further, the absolute minimum becomes the point nearer to the MBH, and  $x_{\min}$  jumps from the green to the red curve. When  $\xi$  increases further, the solution moves out of the triangular region in Figure 6, the absolute minimum of  $f$  remains the inner region, until the minimum becomes again only one (and the  $x_{\min}$  is given again by the black curves). The behavior just described for  $x_{\min}$  also explains why  $x_{\min}$  is so small (similar to that of classical Bondi accretion) in Figure 1, left panel: the values of  $\mathcal{R} = 10^3$  and  $\xi = 100$  in Figure 1 correspond to the red solid curve in Figure 3, i.e., to the regime of very low values for  $x_{\min}$ .

The colors of the curves in the right panel reflect the fact that  $\ln \lambda_t = f(x_{\min}) - 1/2$  and are thus explained by the behavior of  $x_{\min}$  described above. The curves for  $\lambda_t$  are continuous and do not show jumps because  $f(x_{\min})$  decreases continuously for increasing  $\xi$ . For any fixed  $\xi$ , at fixed  $\mathcal{R}$ ,  $\lambda_t$  increases as  $\mathcal{R}$  increases, i.e., as the galaxy mass increases.

As for the Jaffe model, cases with  $\chi < 1$  would have very small differences from the curves in Figure 3, and could be

distinguished only for very large  $\xi$  or small  $\mathcal{R}$ , i.e., when the gravity of the MBH dominates.

## 5. An Application: Evaluation of the Mass Accretion Rate

As an application of the previous results, we investigate here the use of the classical Bondi solution in the interpretation of observational results, in numerical investigations, or in cosmological simulations involving galaxies and accretion on their central MBHs (see Section 1). In many such studies, when the instrumental resolution is limited, or the numerical resolution is inadequate, an estimate of the mass accretion rate is derived using the classical Bondi solution, taking values of temperature and density measured at some finite distance from the MBH. This procedure clearly produces an estimate that can depart from the true value, even when assuming that accretion fulfills the hypotheses of the Bondi model (stationarity, spherical symmetry, etc.). KCP16 developed the analytical setup of the problem for generic polytropic accretion from classical Bondi accretion to the inclusion of the additional effects of radiation pressure and of a Hernquist galactic potential; they also numerically investigated the size of the deviation for some representative cases. Here we reconsider the problem for the isothermal case that was not discussed in detail in KCP16, exploiting our analytical solution, and extending the investigation also to the case of the Jaffe potential.

We briefly start with the case of critical accretion in the classical Bondi problem. For assigned values of  $\rho_\infty$ ,  $T_\infty$ ,  $\gamma$ , and  $M_{\text{BH}}$ , the Bondi radius and accretion rate are given by Equations (6) and (8),

$$r_{\text{B}} = \frac{GM_{\text{BH}}}{c_\infty^2}, \quad \dot{M}_{\text{B}} = 4\pi r_{\text{B}}^2 \lambda_{\text{cr}} \rho_\infty c_\infty. \quad (45)$$

When one inserts in Equation (45) the values of  $\rho(r)$  and  $T(r)$  at a finite distance  $r$  from the MBH, taken along the classical Bondi solution (Section 2.1), and considers them as “proxies” for  $\rho_\infty$  and  $T_\infty$ , then an *estimated* value of the accretion radius ( $r_{\text{e}}$ ) and mass accretion rate ( $\dot{M}_{\text{e}}$ ) is obtained:

$$r_{\text{e}}(r) \equiv \frac{GM_{\text{BH}}}{c_s^2(r)}, \quad \dot{M}_{\text{e}}(r) \equiv 4\pi r_{\text{e}}^2(r) \lambda_{\text{cr}} \rho(r) c_s(r). \quad (46)$$

For theoretical investigations and observational works it is of obvious interest to know how much these  $r_{\text{e}}$  and  $\dot{M}_{\text{e}}$  depart from the true values  $r_{\text{B}}$  and  $\dot{M}_{\text{B}}$  as a function of  $r$ , under the assumption that the Bondi solution holds at all radii.

For  $\gamma = 1$ , the isothermal case of present interest, the sound speed is constant, with  $c_s(r) = c_\infty$ , and then  $r_{\text{e}}(r) = r_{\text{B}}$ , independently of the distance from the center at which the temperature is evaluated. Also,  $\dot{M}_{\text{e}}(r) = 4\pi r_{\text{B}}^2 \lambda_{\text{cr}} \rho(r) c_\infty$ ; at infinity, the estimate coincides<sup>2</sup> with the true value:  $\dot{M}_{\text{e}} = \dot{M}_{\text{B}}$ . At finite radii, from Equations (45) and (46) the deviation of  $\dot{M}_{\text{e}}(r)$  from  $\dot{M}_{\text{B}}$  can be quantified as

$$\frac{\dot{M}_{\text{e}}(r)}{\dot{M}_{\text{B}}} = \tilde{\rho}(x) = \frac{\lambda_{\text{cr}}}{x^2 \mathcal{M}(x)}, \quad (47)$$

<sup>2</sup> Note that in the monoatomic adiabatic case ( $\gamma = 5/3$ ), one instead has that  $\dot{M}_{\text{e}}(r) = \dot{M}_{\text{B}}$  independently of the distance from the center, i.e.,  $\dot{M}_{\text{e}}(r)$  does not deviate from the true accretion rate, while  $r_{\text{e}}(r)$  departs from  $r_{\text{B}}$  (KCP16).

where the last identity derives from Equation (20), and  $\mathcal{M}(x)$  is given in Equation (19). The deviation then is just given by  $\tilde{\rho}(x)$  at the radius  $r$  where the “measure” is taken.

Figure 4 shows the trend of  $\dot{M}_{\text{e}}/\dot{M}_{\text{B}}$  with  $x$  (left panel, for  $\chi = 1$ ). One sees that the use of  $\rho(r)$  instead of  $\rho_\infty$  leads to an overestimate of the true accretion rate  $\dot{M}_{\text{B}}$  at all  $r$ ; however, the overestimate of  $\dot{M}_{\text{B}}$  becomes significant only for  $r < r_{\text{B}}$ .

We next apply the procedure above to the Bondi problem with radiation pressure (Section 3.1). Again  $r_{\text{e}}(r) = r_{\text{B}}$  for  $\gamma = 1$ . We then quantify the difference between the true ( $\dot{M}_{\text{es}} = 4\pi r_{\text{B}}^2 \lambda_{\text{es}} \rho_\infty c_\infty$ , Equation (27)) and estimated ( $\dot{M}_{\text{e}}(r)$  in Equation (46)) accretion rate, with  $\rho(r)$  now evaluated along the Bondi solution including the effect of electron scattering. In this case,

$$\frac{\dot{M}_{\text{e}}(r)}{\dot{M}_{\text{es}}} = \frac{\lambda_{\text{cr}} \tilde{\rho}(x)}{\lambda_{\text{es}}} = \frac{\lambda_{\text{cr}}}{x^2 \mathcal{M}(x)}, \quad (48)$$

where Equation (29) has been used, and  $\mathcal{M}(x)$  is given by Equation (28). Thus now the deviation depends not only on the radius  $r$  where the density is taken, but also on the value of  $\dot{M}_{\text{es}}$  itself through the parameter  $\chi$ , which is included in  $\mathcal{M}(x)$  (see Equation (28)). The trend of  $\dot{M}_{\text{e}}/\dot{M}_{\text{es}}$  as a function of  $x$  is shown in Figure 4, left panel, for two non-special values of  $\chi$ .  $\dot{M}_{\text{e}}$  overestimates the true accretion rate at all radii, even by a large factor if  $r < r_{\text{B}}$ . Of course, the overestimate increases for decreasing  $\chi$ , i.e., for increasing radiation pressure. The size of the overestimate at large radii is given by Equation (48) and Equation (26), which provide  $\dot{M}_{\text{e}}(r) = \tilde{\rho}(x) \dot{M}_{\text{es}}/\chi^2$ , from which  $\dot{M}_{\text{e}}/\dot{M}_{\text{es}} \rightarrow 1/\chi^2$  for  $r \rightarrow \infty$ . The behavior of  $\dot{M}_{\text{e}}/\dot{M}_{\text{es}}$  at small radii is discussed below.

Finally, we evaluate the departure of  $\dot{M}_{\text{e}}(r)$  in Equation (46) from the true mass accretion rate *in presence of a galaxy*, given by  $\dot{M}_{\text{t}} = 4\pi r_{\text{B}}^2 \lambda_{\text{t}} \rho_\infty c_\infty$  (Equation (34)). Taking now  $\rho(r)$  along the solution for accretion within the potential of the galaxy and with electron scattering, one has

$$\frac{\dot{M}_{\text{e}}(r)}{\dot{M}_{\text{t}}} = \frac{\lambda_{\text{cr}} \tilde{\rho}(x)}{\lambda_{\text{t}}} = \frac{\lambda_{\text{cr}}}{x^2 \mathcal{M}(x)}. \quad (49)$$

Figure 4 shows the radial dependence of  $\dot{M}_{\text{e}}/\dot{M}_{\text{t}}$  for the Jaffe and Hernquist galaxy models. Both models have the same  $\mathcal{R} = 10^3$  and the same three values of  $\xi$ ; all differences in the trend of their  $\dot{M}_{\text{e}}/\dot{M}_{\text{t}}$  are then entirely due to the different mass density profiles of these two models. The middle and right panels show a clearly different behavior from that of the left panel (no galaxy):  $\dot{M}_{\text{e}}(r)$  again provides an overestimate for  $r$  taken in the central regions, while  $\dot{M}_{\text{e}}(r)$  becomes a significant *underestimate* for large  $r$ . The position of the radius marking the transition from the region in which there is an overestimate to that where there is an underestimate depends on the specific galaxy model and on the choice of the galaxy parameter values. An important consequence is that, for example, in numerical simulations not resolving  $r_{\text{B}}$ ,  $\dot{M}_{\text{e}}$  should be boosted by a large factor to approximate the true accretion rate  $\dot{M}_{\text{t}}$ . Note that by increasing  $\xi$ , the effect of the Hernquist galaxy becomes more and more similar to that of a single, very high mass concentration, and consequently  $\dot{M}_{\text{e}}$  becomes less and less an underestimate at large radii. For the Jaffe model, this effect is very weak for the parameters of Figure 4.



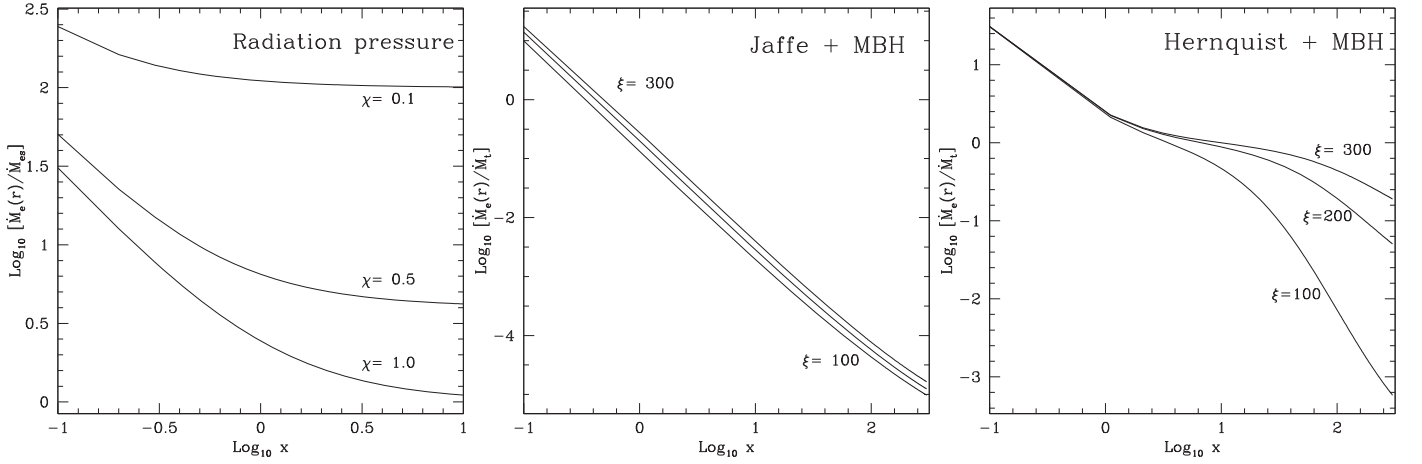


**Figure 4.** Ratio between the estimate of the accretion rate  $\dot{M}_e$  and the true accretion rate ( $\dot{M}_B$ , or  $\dot{M}_{es}$ , or  $\dot{M}_t$ ) as a function of  $x$  (see Section 5). Left: classical Bondi model with the addition of the effect of electron scattering for the three indicated values of  $\chi$ ;  $\chi = 1$  corresponds to classical Bondi accretion. Middle and right: accretion in Jaffe and Hernquist galaxies, with  $\chi = 1$ ,  $\mathcal{R} = 10^3$ , and for three values of  $\xi$ .

It is instructive to find the reason for the common trend of  $\dot{M}_e$  to overestimate the true accretion rate, near the center, in all three panels of Figure 4. This can be achieved from the expansion for  $x \rightarrow 0^+$  of Equation (33), or of the supersonic branch of  $W(-1, z)$  in Equation (35). In both ways, for the galaxy models chosen here and for  $\chi > 0$ , one has that  $\mathcal{M}(x) \sim \sqrt{2\chi}x^{-1/2}$ , and so

$$\frac{\dot{M}_e(r)}{\dot{M}_t} \sim \frac{\lambda_{cr}}{\sqrt{2\chi}x^{3/2}}, \quad x \rightarrow 0^+. \quad (50)$$

This demonstrates that the effect of the galaxy on the ratio  $\dot{M}_e/\dot{M}_t$  disappears for  $x \rightarrow 0^+$ ; and the trend becomes that of the effect of radiation pressure, with the respective value of  $\chi$ . In particular, in Figure 4 all curves in the central region become similar to the curve for  $\chi = 1$  in the left panel (which corresponds to the effect from the pure MBH). Within the range of  $x$  values of Figure 4, the convergence to the classic ( $\chi = 1$ ) Bondi solution has not been reached yet by the Jaffe galaxy, while instead it has been reached by the Hernquist galaxy. This corresponds to the fact that in the central region the galaxy potential is much more important in the Jaffe model than in the Hernquist model. This difference in the galactic potential is also reflected in the different location of the sonic point  $x_{min}$  in the two galaxy models:  $x_{min}$  is very small for the Hernquist galaxy (see Figure 3 for the  $\xi$  values of Figure 4), and it is much larger for the Jaffe galaxy (Figure 2).

For completeness, we also mention the case  $\chi = 0$ . While isothermal stationary accretion is impossible in the Hernquist potential (Section 4.2), for the Jaffe model one has  $\mathcal{M}(x) \sim 2\sqrt{(1 - \mathcal{R}/2\xi)\ln(x/x_{min})}$  for  $x \rightarrow 0$  (provided that  $\mathcal{R} \geq 2\xi$ ). From this expression for  $\mathcal{M}$ , one obtains the analog of Equation (50).

The expansion of  $\mathcal{M}(x)$  for  $x \rightarrow \infty$  explains the trend of  $\dot{M}_e$  at large distances from the MBH. It gives  $\mathcal{M}(x) \sim \lambda_t e^{-(\chi+\mathcal{R})/x}/x^2$ , and then

$$\frac{\dot{M}_e(r)}{\dot{M}_t} \sim \frac{\lambda_{cr}}{\lambda_t}, \quad x \rightarrow \infty. \quad (51)$$

In the case of a galactic potential,  $\lambda_t$  becomes very large, and  $\dot{M}_e/\dot{M}_t$  correspondingly becomes very small, as shown in the

middle and right panels of Figure 4. In particular,  $\lambda_t$  is much larger and less dependent on  $\xi$  for the Jaffe than for the Hernquist model (as shown by Figures 2 and 3). This, together with Equation (51), explains why in Figure 4 the underestimate provided by  $\dot{M}_e$  is much larger for the Jaffe than for the Hernquist galaxy; and why it is hardly dependent on  $\xi$  in the Jaffe case, while it largely varies with  $\xi$  in the Hernquist case.

## 6. Summary and Conclusions

The classical Bondi accretion theory represents the tool commonly adopted in many investigations requiring an estimate of critical quantities as the accretion radius and the mass accretion rate; as examples, we quote here cosmological simulations when the numerical resolution is not high enough to probe the region near the central MBH in a self-consistent way, and the interpretation of observational results when the instrumental resolution does not allow reaching the MBH surroundings. In this work we focused on the case of isothermal accretion in galaxies with central MBHs and with radiation pressure contributed by electron scattering in the optically thin regime. All the hypotheses of classical Bondi accretion (stationarity, absence of rotation, spherical symmetry) are maintained. The radial profile of the Mach number is obtained by using the Lambert–Euler  $W$ -function (commonly implemented in computer algebra systems). Remarkably, for the Jaffe and Hernquist galaxies, we showed that the value of the critical accretion parameter can be analytically calculated. These two facts allow deriving a fully analytical solution for the problem of accretion onto an MBH at the center of galaxies. As an application, we examined the problem of the bias induced on the estimates of the mass accretion rate by the adoption of the classical Bondi solution for accretion on an MBH, and of the gas density and temperature at some finite distance from the center as proxies for their values at infinity. The main results of this work can be summarized as follows.

- (1) For isothermal accretion toward the center of a generic spherically symmetric potential and for a given accretion parameter, the Mach number profile can be written in terms of the  $W$ -function. The dependence of the critical accretion parameter from the properties of the Jaffe and

Hernquist galaxy models with a central MBH is given analytically, even in presence of radiation pressure.

- (2) For the Jaffe potential, the determination of the critical accretion parameter involves the solution of a quadratic equation, and there is only one sonic point for any choice of the parameters describing the galaxy. Moreover, accretion is possible even in absence of the central MBH (for a subset of values of the galaxy parameters).
- (3) For the Hernquist galaxy model, the critical accretion parameter is given by the solution of a cubic equation that is fully investigated; one or two sonic points can be present. It is also shown that isothermal accretion is not possible in a Hernquist galaxy without a central MBH.
- (4) The structure of the accretion flow is sensitive to the mass density profile of the host galaxy; surprisingly, it turned out to be quite different even for the two chosen galaxy models, belonging to the class of  $\gamma$ -models, at fixed total mass and scale length. In fact, in a Jaffe galaxy, the position of the sonic point depends smoothly on the galaxy properties; conversely, in the Hernquist potential, the flow structure is more complex, and the position of the sonic point can jump from very large to very small distances from the center, even for a smooth variation of the galaxy parameters. For example, for the same (plausible) values of the galaxy parameters, the position of the sonic point is  $\approx 400 r_B$  for the Jaffe model and just  $\approx r_B$  for the Hernquist one.
- (5) The size of the departure from the true value of estimates of the accretion rate  $\dot{M}_e(r)$  based on the classical Bondi solution and the gas properties at a finite distance  $r$  from the center is given as a function of this distance. The departure is proportional to the local density of the accreting material. We derived the formulae for the deviation of  $\dot{M}_e(r)$  for the three cases of classical Bondi accretion, of accretion with electron scattering, and of accretion onto an MBH at the center of a galaxy with electron scattering (when the true rate is  $\dot{M}_B$ ,  $\dot{M}_{es}$ , and  $\dot{M}_t$ , respectively).
- (6)  $\dot{M}_e(r)$  is an overestimate of  $\dot{M}_B$ , regardless of the radius at which the density is taken.  $\dot{M}_e(r)$  is always an even larger overestimate of  $\dot{M}_{es}$  when radiation pressure is present; of course, the overestimate becomes larger for increasing radiation pressure. In presence of a galaxy,  $\dot{M}_e(r)$  overestimates  $\dot{M}_t$ , if the density is taken in the central region, and *underestimates*  $\dot{M}_t$  if it is taken outside a few Bondi radii. The size of the overestimate, approaching the center, becomes less and less dependent on the galaxy profile, and close to that of the classical Bondi problem; the size of the underestimate is instead very sensitive to the details of the galaxy profile. A quantitative explanation for these two trends was given. The position of the transition between the two kinds of departures depends on the details of the density profile of the galaxy. In conclusion, caution should be exerted when proposing general recipes for the mass supply rate to the MBH.

Finally, we note that the present investigation can be expanded in an interesting respect, considering the link between the gas temperature and the galaxy properties. In fact, in the present study we kept  $c_\infty$  as a free parameter, while in a galaxy, the gas temperature is likely linked to the depth of the potential well (i.e., it should be close to the virial temperature

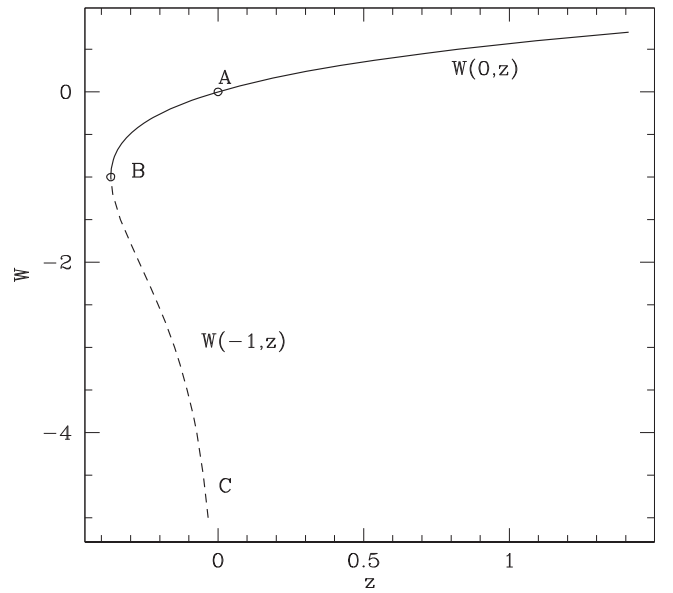


**Figure 5.** Real determination of the  $W$ -function. The two branches involved in the solution of the accretion problem are that of  $W(0, z)$  (solid line) between the points  $A = (0, 0)$  and  $B = (-1/e, -1)$ , and of  $W(-1, z)$  (dashed line) between the points  $B$  and the asymptotic point  $C = (0, -\infty)$ .

of the system). This means that  $r_B$  should depend on  $r_g$  and  $M_g$ , which introduces a physical scale in the problem. Remarkably, the link between the temperature and the potential can be expressed analytically for the two-component (stars + dark matter) Jaffe models with a central MBH (Ciotti & Ziaee Lorzad 2017); this will be the subject of a forthcoming work.

We thank the referee and Daniel Proga for useful comments.

## Appendix A The Lambert–Euler $W$ -Function

The Lambert–Euler function  $W(z)$  is a multivalued complex function implicitly defined by

$$W \exp(W) = z, \quad (52)$$

where in general  $z$  is a complex variable. As is well known, several transcendental equations can be recast and solved in terms of  $W$ . For example, it can be shown that the equation

$$a X^b + c + d \ln X = Y, \quad (53)$$

for the non-negative unknown  $X$ , and where  $a, b, c, d$ , and  $Y$  are quantities independent of  $X$ , has the solution

$$X^b = \frac{d}{ab} W \left[ \frac{ab}{d} \exp \frac{(Y - c)b}{d} \right]. \quad (54)$$

The real determination of  $W$  is shown in Figure 5, and it is made of two branches, called  $W(0, z)$  and  $W(-1, z)$ . For a general discussion of the properties of the  $W$ -function, we refer to the classical papers (e.g., Corless et al. 1996).

The result above shows that Equation (19) gives the required solution to the problem in Section 2, as detailed in Section 2.1.

## Appendix B

### The Critical Parameter for Isothermal Accretion in Jaffe and Hernquist Models with a Central BH

From the discussion in Section 2, it follows that the critical value of the isothermal accretion parameter in the generalized Bondi theory is given by Equation (15). Therefore,  $\lambda_{\text{cr}}$  can be computed explicitly when  $f_{\text{min}}$  is: in turn, this reduces to the determination of  $x_{\text{min}}$ , i.e., the position of the *absolute* minimum of  $f$  for  $x \geq 0$ . In presence of a generic galaxy potential, this is not possible analytically, but in KCP16 it was shown that, quite remarkably, this can be done for the Hernquist model with a central BH in the general polytropic case with electron scattering by solving a cubic equation. For simplicity, the explicit solution was not given, although all the needed information to determine the number and position of the critical points of  $f$  were reported and discussed. Here we give the explicit solution for the Jaffe and Hernquist galaxy models in the isothermal case and electron scattering.

#### B.1. The Jaffe Model

At variance with the Hernquist model, where  $x_{\text{min}}$  (and so  $f_{\text{min}}$  and  $\lambda_t$ ) can be computed analytically for  $1 \leq \gamma \leq 5/3$  (KCP16), in the Jaffe case, the explicit expression of  $x_{\text{min}}$  can be obtained only in the isothermal case,  $\gamma = 1$ . In this case, however, the situation is much simpler than for the Hernquist model. In fact, independently of the value of the galaxy parameters, there is only a single minimum, as can be proved by a study of Equation (37):

$$f' = \frac{2g(x)}{x^2(\xi + x)}, \quad g = x^2 - \frac{\mathcal{R} + \chi - 2\xi}{2}x - \frac{\chi\xi}{2}. \quad (55)$$

The discriminant of the function  $g$  is non-negative for all physical (i.e., positive) values of  $\mathcal{R}$ ,  $\xi$ , and  $\chi$ , so that  $f'$  has two real solutions. Moreover, the Descartes sign rule shows that for  $\xi > 0$  and  $\chi > 0$ , one solution of  $g = 0$  is negative and one is positive, corresponding to the searched position of the minimum of  $f$ ,

$$x_{\text{min}} = \frac{\mathcal{R} + \chi - 2\xi + \sqrt{(\mathcal{R} + \chi - 2\xi)^2 + 8\chi\xi}}{4}. \quad (56)$$

In the peculiar case of  $\chi = 0$  (i.e., when radiation pressure exactly cancels the gravitational field of the BH, and the effective potential is only due to the galaxy), a solution of the accretion problem is possible only for  $\mathcal{R} \geq 2\xi$ , with  $x_{\text{min}}$  and  $\lambda_t$  given in Section 4.1. When  $\mathcal{R} \leq 2\xi$ , the function  $g$  in Equation (55) is positive for  $x > 0$ , so that the minimum is attained at the origin. When  $\mathcal{R} = 2\xi$ , we have  $x_{\text{min}} = 0$  (the sonic point is at the origin),  $f_{\text{min}} = 2 \ln \xi$ , so that it is *finite*, and  $\lambda_t = \xi^2/\sqrt{e}$ , consistent with the limit of  $\lambda_t$  for  $\mathcal{R} \rightarrow 2\xi$  in Equation (42). For  $\mathcal{R} < 2\xi$ ,  $f_{\text{min}} = -\infty$ , and so no accretion is possible because one would derive  $\lambda_t = 0$ . These different behaviors for the Jaffe model with  $\chi = 0$  arise because the galaxy potential is logarithmic, with the possibility to “compensate” near the origin (at least for some choices of  $\mathcal{R}$  and  $\xi$ ) the term  $2 \ln x$ , even in absence of the gravitational field of the MBH. As we will see, the more “regular” nature of the Hernquist potential at the center makes this impossible, and no accretion can take place in the isothermal case for  $\chi = 0$ , independently of the galaxy parameters.

#### B.2. The Hernquist Model

In case of isothermal accretion in a Hernquist galaxy with central BH and radiation pressure due to electron scattering, the critical points of  $f$  are placed at the non-negative zeroes of

$$f' = \frac{2g(x)}{x^2(\xi + x)^2},$$

$$g = x^3 - \frac{\mathcal{R} + \chi - 4\xi}{2}x^2 + \xi(\xi - \chi)x - \frac{\xi^2\chi}{2}. \quad (57)$$

The limiting cases of  $\xi = 0$  and  $\chi = 0$  are discussed in Section 4.2; here we discuss the more realistic case of  $\xi > 0$  and  $\chi > 0$ . The constant term for  $g$  in Equation (57) is strictly negative, while the coefficient of the cubic term is positive; thus,  $f$  has always at least one minimum for  $x > 0$ . However,  $g$  can have three real zeros for some particular values of  $\mathcal{R}$ ,  $\xi$ , and  $\chi$ . It is therefore important to have quantitative criteria to determine the number and position of the critical points of  $f$ , and in particular, of the absolute minimum  $f_{\text{min}}$  that is required.

The existence and the position of the zeros of  $g$  for assigned values of the parameters can be determined from the theory of cubic equations as follows. With the substitution

$$x = z + \frac{\mathcal{R} + \chi - 4\xi}{6}, \quad (58)$$

the function  $g(x)$  in Equation (57) reduces to the canonical depressed form  $g_c(z) = z^3 + pz + q$ , with

$$p = -\frac{\mathcal{R}^2 - 2\mathcal{R}(4\xi - \chi) + (2\xi + \chi)^2}{12},$$

$$q = -\frac{\mathcal{R}^3 - 3\mathcal{R}^2(4\xi - \chi) + 3\mathcal{R}(10\xi^2 - 2\xi\chi + \chi^2) + (2\xi + \chi)^3}{108}, \quad (59)$$

so that once the zeroes  $z_k$  ( $k = 0, 1, 2$ ) of  $g_c(z)$  are known, the corresponding solutions  $x_k$  of  $g(x)$  are obtained from Equation (58). As is well known, the number of real zeros of a cubic equation with real coefficients is determined by the sign of the function

$$R \equiv \frac{q^2}{4} + \frac{p^3}{27}$$

$$= \frac{\xi^2\mathcal{R}[\chi\mathcal{R}^2 - (\xi^2 + 10\chi\xi - 2\chi^2)\mathcal{R} + (2\xi + \chi)^3]}{432}, \quad (60)$$

where the last expression is obtained from Equation (59). This expression can also be obtained from the more general Equation (C4) in KCP16, evaluated for  $\gamma = 1$ .

All the roots appearing in the following equations must be intended as arithmetic roots. When  $R > 0$ , there is only one real solution, given by

$$z_0 = \sqrt[3]{\sqrt{R} - q/2} - \frac{p/3}{\sqrt[3]{\sqrt{R} - q/2}}, \quad (61)$$

and so  $z_0$  determines the location of the only minimum of  $f$ , i.e.,  $x_{\text{min}} = x_0$ . By inspection of Equation (60), it follows that  $R > 0$  both for low and high values of  $\mathcal{R}$  at fixed  $\xi$ , and for low and high values of  $\xi$  at fixed  $\mathcal{R}$ . The exact boundary of the

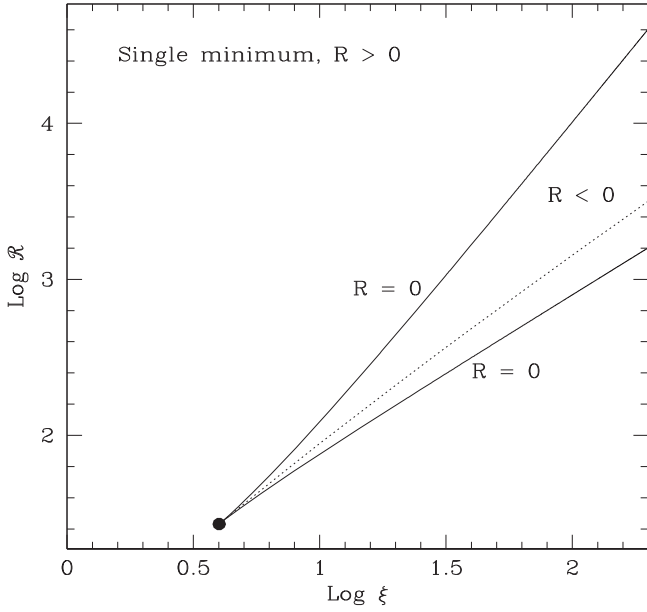


**Figure 6.** Sign of  $R$  in Equation (60) across the  $(\mathcal{R}, \xi)$  plane for Hernquist galaxies in the illustrative case  $\chi = 1$ . The two solid lines correspond to Equation (62), and start at  $(\xi, \mathcal{R}) = (4\chi, 27\chi)$ . For  $\xi$  and  $\mathcal{R}$  within the triangular region defined by the two solid lines, there are two minima and one maximum for  $f$  in Equation (43). Along the dotted line are two sonic points for the accretion flow, since the two minima of  $f$  have the same depth.

region in the  $(\xi, \mathcal{R})$  plane corresponding to  $R > 0$  can be determined rigorously. In fact, for  $\xi < 4\chi$  the discriminant of the quadratic function of  $\mathcal{R}$  in Equation (60) is negative, and so  $R > 0$  independently of the value of  $\mathcal{R}$ . For  $\xi \geq 4\chi$ , in accordance with the Descartes sign rule, there are two positive values of  $\mathcal{R}$ :

$$\mathcal{R}_{\min, \max} = \frac{\xi^2 + 10\chi\xi - 2\chi^2 \pm \sqrt{\xi(\xi - 4\chi)^3}}{2\chi}, \quad (62)$$

so that  $R < 0$  for  $\mathcal{R}_{\min} < \mathcal{R} < \mathcal{R}_{\max}$ , and  $R > 0$  outside this range. Therefore, all points outside the open triangular region in Figure 6 correspond to models with a single minimum for  $f$ , given by Equations (58) and (61). Note that for  $\xi \rightarrow \infty$ ,  $\mathcal{R}_{\min} \sim 8\xi$  and  $\mathcal{R}_{\max} \sim \xi^2/\chi$ .

Along the two critical curves defined by Equation (62) in Figure 6,  $R = 0$  and  $g_c(z)$  has a single real root and a double (and so also real) root, given respectively by

$$z_0 = \frac{3q}{p}, \quad z_{1,2} = -\frac{z_0}{2}. \quad (63)$$

The positions of the associated zeros of  $g(x)$  are given by a surprisingly simple expression. In fact, along the lower solid curve in Figure 6, when  $\mathcal{R} = \mathcal{R}_{\min}$ , one has that

$$0 < x_0 = \frac{\xi[\xi - 2\chi - \sqrt{\xi(\xi - 4\chi)}]}{4\chi} \\ \leq x_{1,2} = \frac{\xi + \sqrt{\xi(\xi - 4\chi)}}{2}, \quad (64)$$

while for  $\mathcal{R} = \mathcal{R}_{\max}$  (the upper solid curve in Figure 6) one has that

$$0 < x_{1,2} = \frac{\xi - \sqrt{\xi(\xi - 4\chi)}}{2} \\ \leq x_0 = \frac{\xi[\xi - 2\chi + \sqrt{\xi(\xi - 4\chi)}]}{4\chi}. \quad (65)$$

In both cases, being  $x_{1,2}$  a double root,  $f$  has an *inflection* point there, and the only minimum is placed at  $x_{\min} = x_0$  given in Equations (64)–(65).

When  $\xi = 4\chi$  (and so  $\mathcal{R} = 27\chi$ ), all solutions collapse (large dot in Figure 6), and there is only a third-order minimum, placed at

$$x_{\min} = x_0 = x_1 = x_2 = 2\chi, \quad f_{\min} = 5 + 2\ln(2\chi) \quad (66)$$

where the last identity follows from Equation (43). Note that  $f_{\min} \rightarrow -\infty$  and  $\lambda_{\text{cr}} \rightarrow 0$  for  $\chi \rightarrow 0$ .

For  $R < 0$  (when necessarily  $p < 0$  from Equation (60)), i.e., for  $\mathcal{R}_{\min} < \mathcal{R} < \mathcal{R}_{\max}$ , there are three real roots of  $g_c(z)$ , given by

$$z_k = 2\sqrt{-\frac{p}{3}} \cos\left(\frac{\varphi}{3} + \frac{2\pi k}{3}\right), \quad k = 0, 1, 2 \quad (67)$$

with

$$0 \leq \varphi \equiv \arccos\left(-\frac{q}{2}\sqrt{-\frac{27}{p^3}}\right) \leq \pi. \quad (68)$$

It is simple to prove that  $z_1 < z_2 < z_0$ ; moreover, the Descartes sign rule applied to Equation (57) with  $\mathcal{R}_{\min} < \mathcal{R} < \mathcal{R}_{\max}$  shows that the three real zeros are positive, so that, from Equation (58),  $x_1$ ,  $x_2$ , and  $x_0$  correspond to a minimum, a maximum, and a minimum of  $f$ , respectively. In the case  $R < 0$ , we must then determine the position of the absolute minimum among  $x_1$  and  $x_0$ . This is illustrated by the following procedure.

Assume we fix a value of  $\xi > 4\chi$  and we start increasing  $\mathcal{R}$  from a very low value, i.e., we move vertically in the plane of Figure 6. Initially, there is only one minimum  $x_{\min} = x_0$  given by Equation (61), so that  $f$  increases monotonically for  $x > x_0$ . When  $\mathcal{R}$  reaches the lower curve  $R = 0$  ( $\mathcal{R} = \mathcal{R}_{\min}$ ), a double root  $x_{1,2}$  appears, corresponding to an inflection point of  $f$ , while  $x_{\min} = x_0$ , as in Equation (64). For  $\mathcal{R}_{\min} < \mathcal{R} < \mathcal{R}_{\max}$ , now  $R < 0$ , the double root splits, and Equation (67) applies. The absolute minimum corresponds to  $z_1$ , while  $z_2$  and  $z_0$  correspond to a maximum and a minimum of  $f$ , respectively. Increasing  $\mathcal{R}$  further,  $z_2$  moves toward  $z_1$ , while the minimum corresponding to  $z_0$  deepens; when the dotted curve is reached, the two minima of  $f$  have the same value, i.e.,  $f(x_1) = f(x_0)$ , and the accretion flow has two sonic points. Above the dotted curve, the absolute minimum jumps at  $z_0$ , and the minimum at  $z_1$  becomes less and less pronounced. When  $\mathcal{R} = \mathcal{R}_{\max}$ , the two zeroes  $z_1$  and  $z_2$  merge, so that  $x_{1,2}$  becomes the new inflection point of  $f$ , while the absolute minimum is now at  $x_0$ , again given by Equation (65). For higher values of  $\mathcal{R}$ , there is only one minimum given by Equation (61).

#### ORCID iDs

Luca Ciotti <https://orcid.org/0000-0002-5708-5274>  
 Silvia Pellegrini <https://orcid.org/0000-0002-8974-2996>

## References

- Baganoff, F. K., Maeda, Y., Morris, M., et al. 2003, *ApJ*, 591, 891
- Barai, P., Proga, D., & Nagamine, K. 2011, *MNRAS*, 418, 591
- Barai, P., Proga, D., & Nagamine, K. 2012, *MNRAS*, 424, 728
- Bondi, H. 1952, *MNRAS*, 112, 195
- Bu, D.-F., Yuan, F., Wu, M., & Cuadra, J. 2013, *MNRAS*, 434, 1692
- Cao, X. 2016, *ApJ*, 833, 30
- Chandrasekhar, S. 1939, *An Introduction to the Study of Stellar Structure* (Chicago, IL: Univ. Chicago Press)
- Choi, E., Ostriker, J. P., Naab, T., et al. 2017, *ApJ*, 844, 31
- Ciotti, L., & Ostriker, J. P. 2012, in *Hot Interstellar Matter in Elliptical Galaxies*, Vol. 378, ed. D.-W. Kim & S. Pellegrini (New York: Springer), 83
- Ciotti, L., & Ziaee Lorzad, A. 2017, *MNRAS*, submitted (arXiv:1707.08822)
- Corless, R. M., Gonnet, G. H., Hare, D. E. G., et al. 1996, *Adv Comput Math*, 5, 329
- Cranmer, S. R. 2004, *AmJPh*, 72, 11
- DeGraf, C., Dekel, A., Gabor, J., & Bournaud, F. 2017, *MNRAS*, 466, 1462
- Dehnen, W. 1993, *MNRAS*, 265, 250
- Di Matteo, T., Colberg, J., Springel, V., Hernquist, L., & Sijacki, D. 2008, *ApJ*, 676, 33
- Frank, J., King, A., & Raine, D. 1992, *Accretion Power in Astrophysics Vol. 21* (Cambridge: Cambridge Univ. Press)
- Fukue, J. 2001, *PASJ*, 53, 687
- Herbst, R. S. 2015, PhD thesis, Univ. Witwatersrand
- Hernquist, L. 1990, *ApJ*, 356, 359
- Hopkins, P., Hernquist, L., Cox, T. J., et al. 2006, *ApJS*, 163, 1
- Hopkins, P., Hernquist, L., Cox, T. J., et al. 2007, *ApJ*, 669, 45
- Jaffe, W. 1983, *MNRAS*, 202, 995
- Kormendy, J., & Ho, L. C. 2013, *ARA&A*, 51, 511
- Kormendy, J., & Richstone, D. 1995, *ARA&A*, 33, 581
- Korol, V., Ciotti, L., & Pellegrini, S. 2016, *MNRAS*, 460, 1188 (KCP16)
- Lusso, E., & Ciotti, L. 2011, *A&A*, 525, 115
- Magorrian, J., Tremaine, S., Richstone, D., et al. 1998, *AJ*, 115, 2285
- Park, K., & Ricotti, M. 2011, *ApJ*, 739, 2
- Park, K., Ricotti, M., Natarajan, P., Bogdanovic, T., & Wise, J. H. 2016, *ApJ*, 818, 184
- Park, K.-H., Wise, J. H., & Bogdanović, T. 2017, *ApJ*, in press (arXiv:1704.0786)
- Pellegrini, S. 2005, *ApJ*, 624, 155
- Pellegrini, S. 2010, *ApJ*, 717, 640
- Rafferty, D. A., McNamara, B. R., Nulsen, P. E. J., & Wise, M. W. 2006, *ApJ*, 652, 216
- Russell, H. R., Fabian, A. C., McNamara, B., & Broderick, A. E. 2015, *MNRAS*, 451, 588
- Sijacki, D., Springel, V., Di Matteo, T., & Hernquist, L. 2007, *MNRAS*, 380, 877
- Tremaine, S., Richstone, D. O., Byun, Y.-I., et al. 1994, *AJ*, 107, 634
- Volonteri, M., Capelo, P. R., Netzer, N., et al. 2015, *MNRAS*, 449, 1470
- Waters, T. R., & Proga, D. 2012, *MNRAS*, 426, 2239
- Wong, K.-W., Irwin, J. A., Shcherbakov, R. V., et al. 2014, *ApJ*, 780, 9
- Yuan, F., & Narayan, R. 2014, *ARA&A*, 52, 529